Simulation of telescope detectivity for GEO survey and tracking

Pascal Richard
C.N.E.S.

ABSTRACT

As the number of space debris on earth's orbit increases steadily, the need to survey, track and catalogue them becomes of key importance. In this context, CNES has been using the TAROT Telescopes (Rapid Telescopes for Transient Objects owned and operated by CNRS) for several years to conduct studies about space surveillance and tracking. Today, two testbeds of services using the TAROT telescopes are running every night: one for GEO situational awareness and the second for debris tracking. Additionally to the CNES research activity on space surveillance and tracking domain, an operational collision avoidance service for LEO and GEO satellites is in place at CNES for several years. This service named CAESAR (Conjunction Analysis and Evaluation: Alerts and Recommendations) is used by CNES as well as by external customers. As the optical debris tracking testbed based on TAROT telescopes is the first step toward an operational provider of GEO measures that could be used by CAESAR, simulations have been done to help choosing the sites and types of telescopes that could be added in the GEO survey and debris tracking telescope network. One of the distinctive characteristics of the optical observation of space debris compared to traditional astronomic observation is the need to observe objects at low elevations. The two mains reasons for this are the need to observe the GEO belt from non-equatorial sites and the need to observe debris at longitudes far from the telescope longitude. This paper presents the results of simulations of the detectivity for GEO debris of various telescopes and sites, based on models of the GEO belt, the atmosphere and the instruments. One of the conclusions is that clever detection of faint streaks and spread sources by image processing is one of the major keys to improve the detection of debris on the GEO belt

1. INTRODUCTION

One of the distinctive characteristics of the optical observation of space debris compared to traditional astronomic observation is the need to observe objects at low elevations. The three main reasons for this are the need to observe the GEO belt from non-equatorial sites, the need to observe debris at longitudes far from the telescope longitude and the need to observe GEO debris with inclination.

. Observing from non equatorial sites can be imposed by geographical constraints.

. Observing far from the telescope longitude is useful for tracking of debris on parts of orbit non observable by telescopes at the same longitude of the debris.

The seasonal effect of the inclination of the debris as seen from two different longitudes is presented by Fig. 1.

The simulators presented here have been developed in order to help determine the magnitude limit of a telescope observing faint debris at low elevation.

Paragraph 2 presents the models used in the simulator of space object reflectivity and a validation test case based on observation of Telecom2D satellite by the two Tarot Telescopes presented in [1] and [2].

Paragraph 3 presents the method used for evaluating the detection capability of moving objects considering the relative angular size of pixel and seeing.

Paragraph 4 presents the simulation of detectivity of moving objects for various telescopes and atmospheric conditions.The simulation method used in this paragraph is based on the method presented in [3], adding the considerations about seeing developed in paragraph 3.

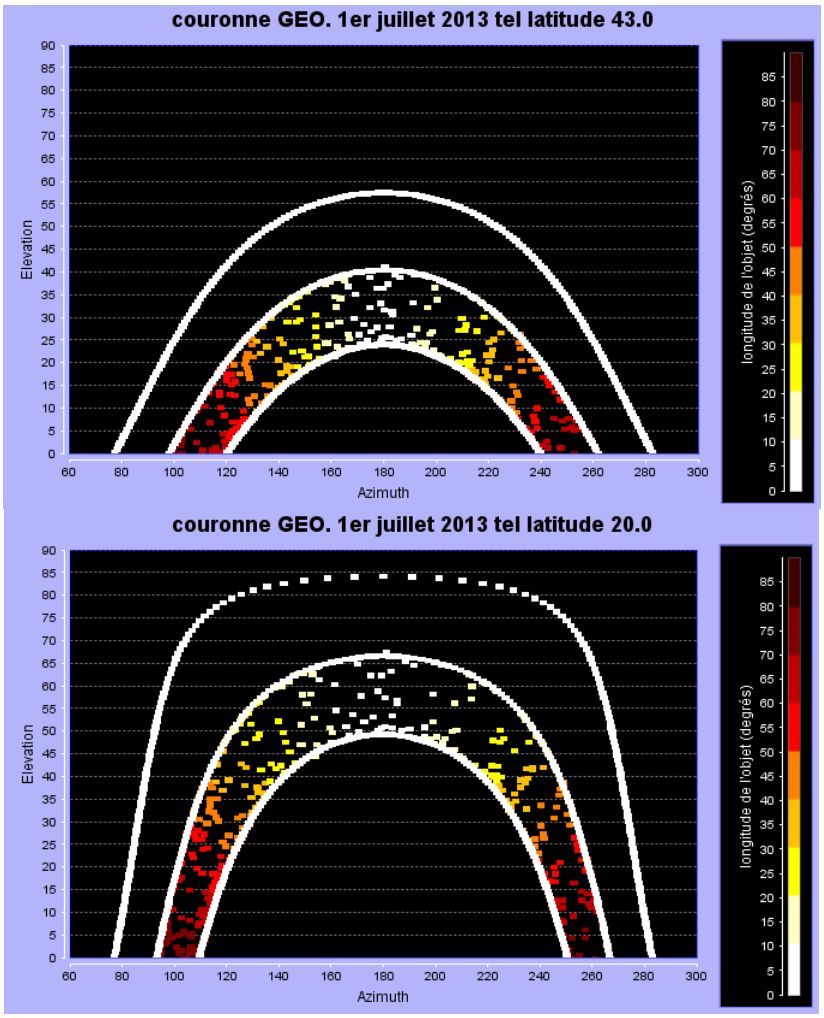

Fig. 1. Azimuth and elevation of the GEO resident objects referenced by SpaceTrack from locations (43°N,0°E) and (20°N,0°E) at the hour of best illumination near summer solstice. The colors indicate the longitude (east or west without distinction) of the objects. The three white lines are (from top to bottom) the highest elevation for 15° inclination GEO objects, the GEO belt and the lowest elevation for 15° inclination GEO objects.

2. REFLECTIVITY MODELS

Three reflectivity models have been introduced in the simulator:

- The Lambert reflection model for diffuse reflection on smooth surfaces [3],
- The Lommel-Seeliger model that is often used for asteroid shape restitution [4]. As a model of diffuse reflection on rough surfaces, it will boost the raking reflection of normal lighting,
- The Phong specular reflection model that is often used in computer graphics [5]. Compared to pure specular reflection, the Phong model spreads the specular reflection, helping to take account of not perfectly plane specular surfaces.

To insure the conservation of energy, normalization factors have been introduced as presented in Table 1.

Table. 1. Reflection models

Type of reflection	**model**	**equation**	**Normalisation factor**
Diffuse reflection on smooth surface	Lambert	$brdf = \frac{1}{2\pi}$	k = 1
Diffuse reflection on rough surface	Lommel-Seeliger	$brdf = \frac{k}{(\cos\iota, n + cosr, n)}$	$k = \frac{1}{2\pi \ln\ 1 + \frac{1}{cos\iota, n}}$
Blunted specular reflection. The larger is alpha, the sharper is the specularity.	Specular Phong	$brdf = k\ cos^{\alpha} r, r_0$	$k = \frac{\alpha + 1}{2\pi}$ Value of *k* is exact for normal lighting. Normalisation is more difficult for raking lighting)

To test the capacity of those models to reproduce real photometric measures, we used a geometrical model of Telecom 2D, a communication GEO satellite located at longitude 8°W and adjusted reflection parameters on the measures obtained with Tarot Calern (TCA, 44°N, 7°E) and Tarot Chili (TCH, 29°S, 71°W) telescopes.

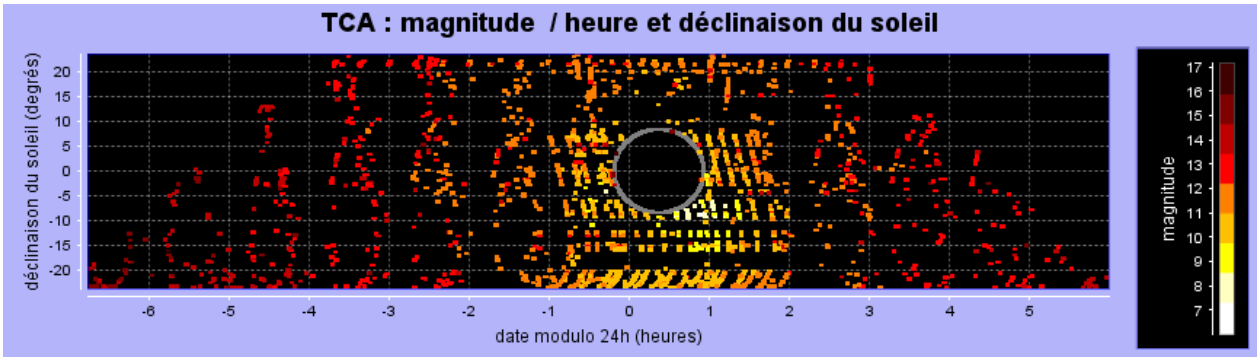

Fig. 2.a : magnitude of the satellite measured by Tarot Calern (TCA) telescope.

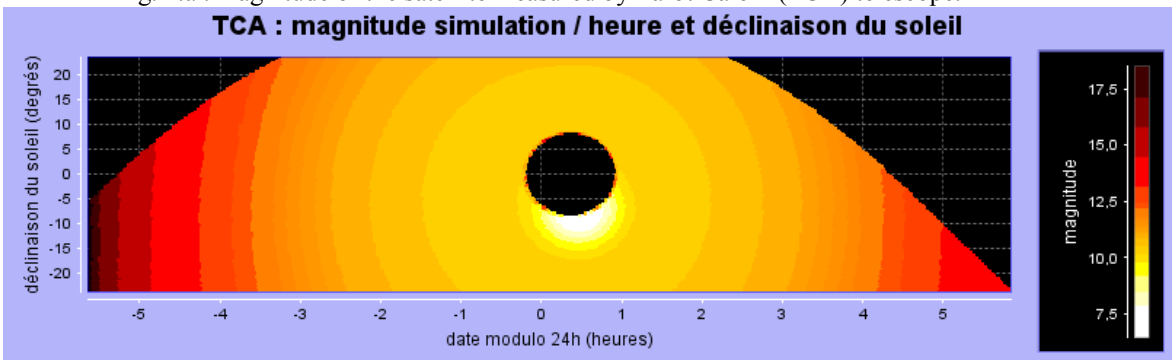

Fig. 2.b : simulation of the magnitude of the satellite as seen by Tarot Calern telescope.

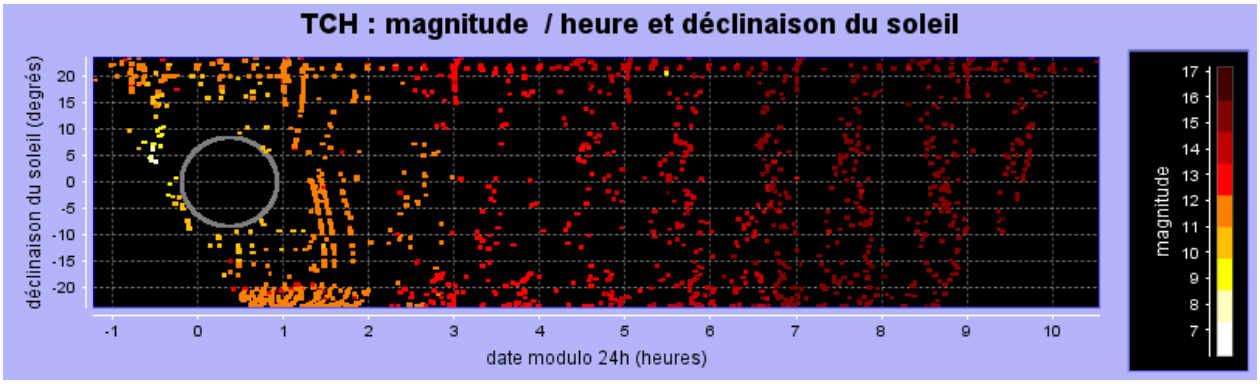

Fig. 2.c: magnitude of the satellite measured by Tarot Chili (TCH) telescope.

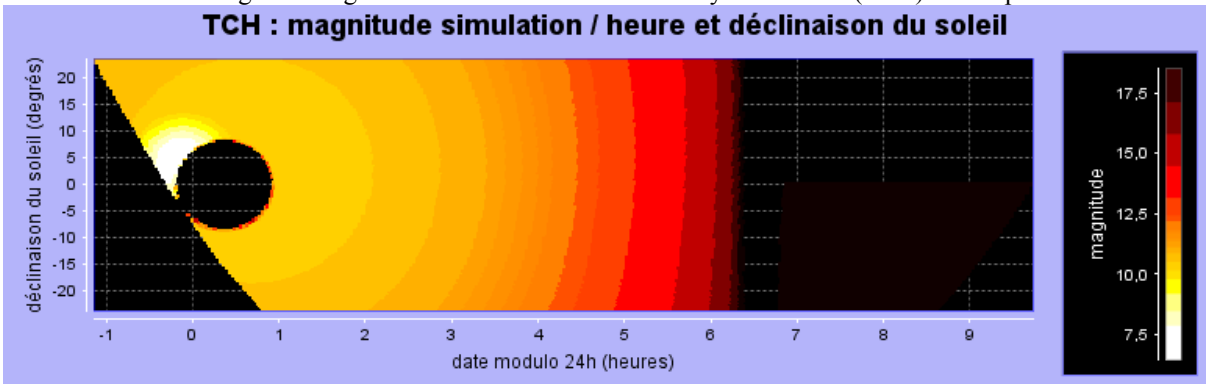

Fig. 2.d: simulation of the magnitude of the satellite as seen by Tarot Chili telescope.

Fig. 2. Magnitude of the GEO satellite as observed by Tarot Calern (TCA) and Tarot Chili (TCH) telescopes. The abscissa and ordinates are respectively the declination of the Sun in degrees and the solar hour.

The results shown in Fig. 2 have been obtained using the parameters presented in Table 2. The Phong specularity model has been chosen instead of the pure specular reflection model to take account of the fact that the real facets of the satellite are not perfectly flat as in our model. The simulation fits correctly the bright and medium measures. However, the Tarot Chili telescope measures after 6:00 a weak residual light that is not reproduced by the model. This lightning could be explained as proposed in [7] by the earthshine illumination of the satellite.

Table 2 : parameters used for the simulation presented in Fig. 2.

Component	Specular reflection ratio	Phong alpha parameter	Diffuse reflection ratio	Main effect
Solar Generator	0,03	384	0.	Adjusted on the very bright measures near eclipse Alpha=384 → almost specular
White nadir antenna	0,6	2	0.	Adjusted on the brightness of the measures between 20 hours and 4 hours. Alpha = 2 → very spread specularity
MLI on east and west faces	???	???	0,1	Diffuse component is visible after midnight at Calern (east face) and before midnight in Chili (west face). The specular component cannot be measured as it is visible only when the sun is above the horizon : at 10:00 from Calern and 15:00 hour from Chili.
North and South optical solar reflectors (OSR)	???	???	0.	Cannot be measured by Tarot telescopes as specularity is visible from earth around noon.

3. EFFECT OF SEEING ON THE DETECTION OF MOVING OBJECTS

An illuminated object crossing the field of view during the exposure will leave a streak on the CCD. A longer exposure will lead to a longer streak and a sky background noise level.

The aim of the method presented here is to determine the optimal streak length as a function of pixel width and seeing FWHM (full width at half maximum) and to determine either the part of the signal received by the best pixel for this optimized streak length.

The part of the signal on the best pixel is determined by discretization of a gaussian PSF (point spread function) and of the exposure time.

The streak length maximizing the signal to noise ratio (SNR) is computed considering that the noise level is proportional to the square root of the exposure time: the read noise is neglected and only the sky background brightness is taken into account. This simplification could have an effect in case of very dark sky and large seeing compared to pixel size.

To simulate the worst case possible, we considered a vertical streak leaved by a debris at the boundary of two columns of pixels and crossing the boundary of two rows at the central date of exposure: even with large pixels and without angular speed of the debris, the maximal part of the signal received by the best pixel is only 25% percent of the signal received by the CCD. This geometry is illustrated by Fig. 3.

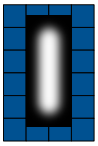

Fig. 3. Geometry of the worst streak on the sensor : the streak is vertical at the boundary of two columns and centered on the boundary of two lines.

The results of those simulations are given by Fig. 4.

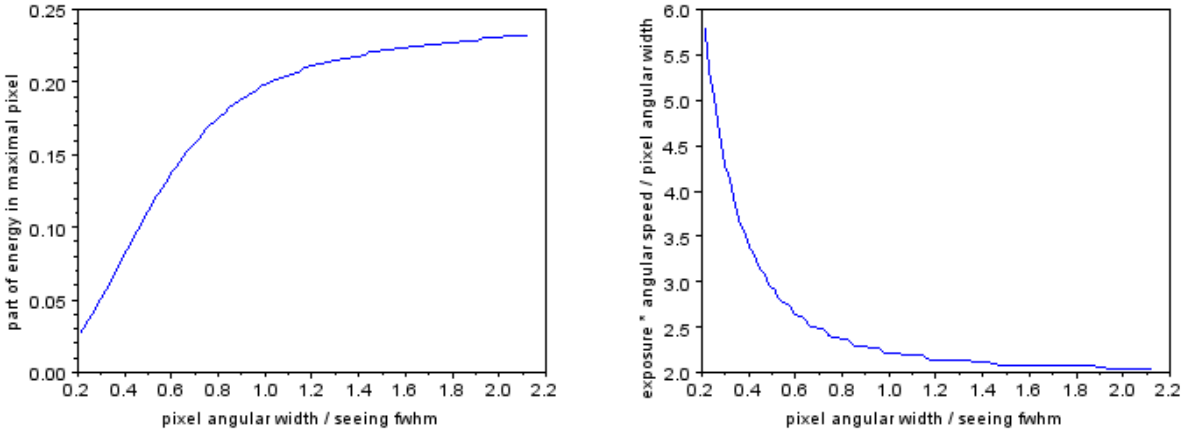

Fig. 4. Results of numerical simulation :
. as the object is at the crossing of four pixels at the central date of the exposure, the maximal ratio of energy reached for very large pixels is 25% with exposure time adjusted for the object to cross two pixels. For very small pixel width, the optimal is obtained with exposure time adjusted for the object to cross 1.1 FWHM.

Two rational approximations have been fitted on this curves for $0 < \frac{pixelWidth}{seeing} < 3.0$:

$$\frac{partInCentralPixel}{\frac{pixelWidth}{seeing}} = \frac{-0.0000759 + 0.00581x + 0.187x^2 + 0.0108x^3}{0.383 - 0.350x + 0.997x^2}$$

$$\frac{\frac{streakLength}{pixelWidth}}{seeing} = \frac{0.262 + 0.179x + 0.618x^2 - 0.0153x^3}{0.214 + 0.255x}$$

4. DETECTIVITY FOR VARIOUS ATMOSPHERIC CONDITIONS

To simulate the detectivity of a telescope taking account of its characteristics, its location, the zenith angle of the observation and the angular velocity of the target, we used a methodology similar to the one presented in [3]. However, the simulation of the effect of seeing has been added for the following reasons: some of the locations considered in our project are not very good astronomic sites, we want to take account of second-rate seeing conditions to maximize the number of usable nights and we want to evaluate what can be done at low elevation above horizon.

The example presented here is based on a classical technic for GEO survey: use of equatorial mount ground telescope without motorization during exposure: stars appear as horizontal streaks, operational geo satellites as dots and GEO debris as short streaks.

The observation chosen for the simulation has been selected as the fastest angular speed for GEO debris crossing the field of view in this survey mode: observation of a 15° inclination GEO debris crossing the equator at about 5''/s.

a. Environmental parameters

To illustrate the effect of the quality of the environment of the telescope, four arbitrary sets of environmental parameters presented in Table 3 have been chosen for the simulations. The background radiance has been set to mag 20 per arcsecond at zenith. This is not a very dark sky, but illustrates the conditions that can be encountered beginning observation before darkest part of the night.

Table 3: sets of environmental parameters

Name of the set	Altitude (m)	Zenithal seeing (arcseconds)	Aerosol optical depth at 550nm
0	0	4	0.20
1000	1000	3	0.15
2000	2000	2	0.10
3000	3000	1	0.05

b. Models

The models used for the simulation are the following:

- Seeing(elevation,zenithal seeing) : approximated by the Kolmogorov and Fried formula for lambda=550nm as presented in [7] :

$$S = S_0 . m^{0.6} . \left(\frac{\lambda}{\lambda_0}\right)^{0.2}$$

- Skybrightness(élévation,zenithal brightness) : as in presented in [3].
- Airmass(élévation) : Rozenberg formula $m = (\cos z + 0.025 e^{-11 \cos z})^{-1}$ where z is the cosine of the zenithal distance as presented in [9],
- Solar brightness at AM0(lambda) : sampled from 0,2 à 1,05 µm by 0,05 µm.
- Atmospheric transmission (wavelength, altitude of the telescope location, atmospheric optical depth (AOD) for 550 nm wavelength, zenithal distance):
  . loss by Rayleigh diffusion as presented in [10],
  . loss by ozone as a function of the wavelength and the zenithal angle as presented in [11] (very few effect),
  . loss by aerosols as a function of the wavelength and the AOD for 550 nm wavelength as used in [12].
- Optimal exposure time and part of the signal in the best pixel: as presented in paragraph 3.
  As the red end of the spectra is better transmitted by atmosphere and less subject to seeing spreading than the 550 nm reference wavelength, the monochromatic values presented in paragraph 3 are biased. After simulations on various atmospheric conditions, it appeared that it is only slightly underestimated : the bias is roughly zero for good atmospheric conditions and up to 10% of the residual central pixel energy for very bad atmospheric conditions (see level, aod=0.4 and elevation 10 degrees above horizon).

c. Télescopes

The results presented if Fig 5 and Fig. 6 are based on the Tarot telescope characteristics and, to allow easier combination of results across publication, the characteristics of theoretical telescopes used in [3]. Thoses characteristics are respectively presented in Table 4 and 5.

Table 4: TAROT telescope characteristics

Primary mirror diameter (mm)	250	
Focal length (mm)	850	
Equivalent diameter for 100% transmission (mm)	145	Taking into account obstruction and optical transmission in autonomous dusty conditions.
Camera	AndorDW436	Characteristics found in [13].

Table 5: Theoretical telescopes

Primary mirror diameter (mm)	250, 500, 1000
f/D	2
transmission	60%
Camera	Pixel size=12 µm Read noise = 8e- quantum efficiency=0.75

d. Results

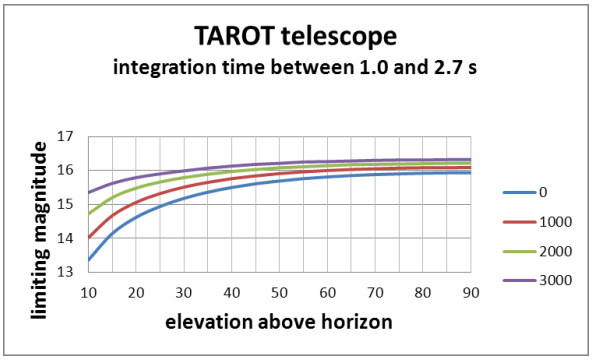

Figure 5: limiting magnitude of Tarot telescope for a 5''/s GEO debris.

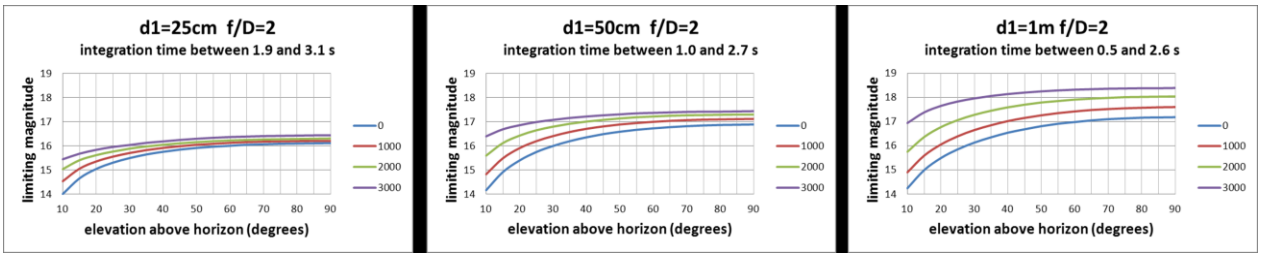

Figure 6: limiting magnitude of three theoretical telescopes for a 5''/s GEO debris.

5. CONCLUSIONS

The detectivity simulations show the amplitude of the loss of detectivity at low elevation for faint moving objects. As the detection algorithm used here is based on a single pixel SNR threshold selected to avoid single dot false detections, the detection of faint streaks below this threshold is not taken into account. The next step will be to simulate the improvement we can get using faint streak detection or image stacking algorithms as presented in [14].

6. REFERENCES

[1] Klotz A., Boër M., Atteia, J.L. and Gendre, B. *Early Optical Observations of Gamma-Ray Bursts by the TAROT Telescopes: Period 2001-2008*, Astron. J., vol. 137, p. 4100, 2009.

[2] Laas-Bourrez M. *Détection des satellites artificiels dans les images astronomiques : application aux images TAROT*, Université de Provence, Marseille, Thèse de Doctorat 2009.

[3] Shell J.R. *Optimizing orbital debris monitoring with optical telescopes*, Amostech 2010.

[4] Lambert J. H. *Photometria, sive de Mensura et Gradibus Luminis, Colorum et Umbrae*, Augsburg, 1760

[5] FairBairn M.B. *Planetary Photometry: The Lommel-Seeliger Law*, 2005JRASC..99...92F

[6] Phong B.T. *Illumination for computer generated pictures*, Commun. ACM 18, 6 (June 1975), 311-317.
[7] Cognion R.L. *Observations and Modeling of GEO Satellites at Large Phase Angles*, Amostech, 2013.
[8] Nestoras J.S. *Photometric observations and data reduction of contact binary systems and of SS433 Long Term study of the astronomical seeing in mount Xolomon Chalkidikis*, Aristotle University of Thessaloniki, 2007.
[9] Rozenberg G.V. *Twilight, a study in atmospheric optics*, Plenum press, 1966.
[10] Hayes D.S. and Latham D.W. *A rediscussion of the atmospheric extinction and the absolute spectral energy distribution of Vega*, 1975ApJ…197..593H.
[11] Lindzen R.S. and Will D.I. An analytical formula for heating due to ozone absorpsion, J. Atmos. Sci., 30, 513–515, 1973
[12] Buil C. http://www.astrosurf.com/buil/extinction/calcul.htm
[13] *Andor Technology DW436/436N/436C*, http://www.andor-tech.com
[14] Yanagisawa T. *Comparison of four detection algorithms for GEO objects*, Amostech, 2012.